Available online at www.sciencedirect.com
ScienceDirect
Trans. Nonferrous Met. Soc. China 34(2024) 1049−1064
Transactions of Nonferrous Metals Society of China
www.tnmsc.cn

Enhancing strength−ductility synergy of AlN_p/Al composite by regulating heterostructure of matrix grain and particle distribution

Yu-yao CHEN[1], Jin-feng NIE[1], Yong FAN[1], Lei GU[1], Ke-wei XIE[2], Xiang-fa LIU[2], Yong-hao ZHAO[1]

1. Nano and Heterogeneous Materials Center, School of Materials Science and Engineering, Nanjing University of Science and Technology, Nanjing 210094, China;
2. Key Laboratory for Liquid−Solid Structural Evolution and Processing of Materials, Ministry of Education, Shandong University, Jinan 250061, China

Received 13 October 2022; accepted 11 May 2023

Abstract: Three heterostructured AlN_p/Al composites with different microstructure configurations were fabricated by liquid−solid reaction combined with subsequent thermal-mechanical treatment to obtain a superior strength and ductility combination. The effects of the microstructure configuration including the AlN particle distribution and matrix grain structure on the tensile strength and ductility were studied in detail. The results show that the simultaneous enhancement of tensile strength and ductility can be achieved. The Uniformed-AlN_p/Al composite with relatively dispersed particles exhibits a superior ultimate tensile strength of ~387 MPa with an elongation to failure of ~9.1%. It shows an outstanding specific tensile strength and elongation combination compared with other reported particle reinforced aluminum matrix composites. Furthermore, the hetero-deformation induced (HDI) stress has been calculated and is shown to increase significantly in the Uniformed-AlN_p/Al composite. It is revealed that the HDI stress plays a crucial role in the significant enhancement of strength and ductility for the AlN_p/Al composite.

Key words: AlN_p/Al composite; tensile strength; ductility; heterogeneous structure; particle distribution; strengthening mechanism

1 Introduction

Particle reinforced aluminum matrix composites (PRAMCs) beneficially combine the advantages of both aluminum matrix and reinforcement particles, including high specific strength, high specific modulus, good wear resistance and so on, and exhibit wide application prospects in the fields of aerospace and automobile industry. With the rapid development of clean energy, the demand for lightweight alloys, especially aluminum alloy and aluminum matrix composite, is also increasing rapidly [1,2]. PRAMCs are the most economical and promising candidates in automotive industries and aerospace that can improve energy efficiency and reduce emissions. However, the tradeoff between the strength and ductility of PRAMCs severely limits their application. At present, simultaneously enhancing the strength and ductility of PRAMCs is still a long-standing challenge, and thus new strategies based on the microstructure design have been proposed [3,4].

It is well known that adding ceramic particles (e.g., TiC, TiB_2, and Al_2O_3) into an aluminum matrix can effectively improve the stiffness and strength of composites [5−8]. Moreover, the mechanical properties of the composites are significantly influenced by the type, size, volume

Corresponding author: Jin-feng NIE, Tel: +86-25-84303281, E-mail: niejinfeng@njust.edu.cn;
Yong-hao ZHAO, Tel: +86-25-84315304, E-mail: yhzhao@njust.edu.cn
DOI: 10.1016/S1003-6326(23)66453-2

fraction of the particles and the interface bonding strength between the particle and the matrix [9,10]. In particular, it is found that the spatial configuration of the reinforcement particles plays a crucial role. The strength and ductility can be effectively enhanced by regulating the spatial configuration of particles [11−13]. For example, SCHERM et al [14] prepared Al_2O_3 reinforced Al−9Si−3Cu composites with a network structure, and found that the elastic modulus and tensile strength were two times higher than those of the matrix alloy, respectively. In addition, when the reinforcement particles are distributed along the grain boundaries and formed a network structure, the grain boundaries can be further strengthened and can effectively impede the intragranular dislocation movement. MIRACLE et al [15] prepared SiC/7095Al composites with laminated distributed particles and found that the toughness of the composite was significantly improved while maintaining the high strength and stiffness of the composites. Therefore, the spatial configuration of reinforced particles in the composites has been proven to play a crucial role in the enhancement of comprehensive mechanical properties.

Recently, heterostructured (HS) materials as a fast-emerging field have attracted increasing attention. HS materials are defined as materials containing heterogeneous zones with dramatically different constitutive properties in the case of structural metallic materials [16,17]. HS materials usually include several types, such as heterogeneous lamella structure, bimodal structure, harmonic structure, gradient structure, etc [18]. It has been proved that the strength and ductility of traditional materials can be simultaneously improved by introducing a heterogeneous structure [19−21]. For example, GENG et al [6] prepared hierarchically structured Al−Mg−Si alloys/nanocomposites by utilizing the accumulative roll bonding process, and the laminated structure was composed of layered distribution of TiC nanoparticles, bimodal-sized grains and precipitates. Compared with a single TiC_p/Al−Mg−Si composite, the yield strength and uniform elongation of the laminated Al−Mg−Si alloys/nanocomposites were increased from 380 MPa and 5.0% to 443 MPa and 6.4%, respectively. Therefore, it can be expected that the synergy of the strength and ductility of the PRAMC can be further enhanced by regulating the spatial configuration of the reinforced particles and the heterostructure of the matrix.

Generally, during plastic deformation treatment, such as extrusion, rolling, high pressure torsion, equal channel angular pressing and accumulative roll bonding, large plastic deformation will be accumulated in materials, which can be used to regulate heterogeneous microstructure [22,23]. In our previous work, an Al−(TiB_2+TiC)/6063 composite with a lamellar structure was successfully prepared by the accumulative rolling method [24], which exhibited a good combination of strength and ductility. At the same time, plastic deformation can disperse particle clusters and regulate the configuration of particles in the matrix. For example, JIANG et al [25] obtained a microstructure characterized with fiber-like nanoparticle-rich zones that contain spherical nanoparticles of boron carbide in an ultrafine grained aluminum alloy matrix. This microstructure was synthesized by cryomilling combined with the hot-extrusion method. However, there are few studies about the effects of particle configuration on the tensile properties of a heterostructured aluminum matrix composite. Considering that nanoparticles can significantly refine the grain size of the Al matrix and have a significant influence on dislocations, it is feasible to achieve a heterogeneous structure of the matrix by regulating the particle configuration. It is hoped that the strength of aluminum matrix composites can be improved without sacrificing ductility by introducing heterogeneous structures.

In this work, a new strategy was proposed to improve the strength and ductility synergy of PRAMCs by regulating the particle configuration and the heterogeneous microstructure. A heterostructured AlN_p/Al composite was fabricated by liquid−solid reaction combined with the subsequent thermal-mechanical treatment. The lamellar heterostructure of matrix grains was regulated by the thermo-mechanical deformation. Meanwhile, different particle configurations were also obtained due to the evolution of particle distribution during plastic deformation. The effects of particle configurations on the tensile properties of the heterostructured composite were revealed and the strengthening mechanisms were also discussed in depth. The proposed strategy will provide new insight and guidance for the design of composites with superior strength and ductility combinations.

2 Experimental

2.1 Fabrication of AlN_p/Al composite

Figure 1 shows the fabrication process of the heterostructured AlN_p/Al composite in the present study. Commercially pure Al powders (99.7%, all compositions quoted in this work are nominal values in mass fractions unless otherwise stated) and nitride plastid powders (referred to as N_P, 99%) were used. In this study, a two-step ball-milling method was utilized to regulate the microstructure. Firstly, in Step I, pure Al powders and N_P were mixed uniformly and N_P was attached to the surface of Al powders during the ball-milling process with a rotation speed of 200 r/min and a ball-to-powder ratio of approximately 20:1 to obtain the N_P/Al precursor powders. Secondly, the pure Al powders with the N_P/Al powders obtained in Step I were further ball-milled to form reinforcement particle rich zones and particle poor zones in Step II. Then, during the subsequent sintering process, the nitrogen atoms from N_P diffused into the surface of aluminum powders and reacted with Al atoms to form AlN nanoparticles, that is, the AlN particles (AlN_p) were in-situ formed in the aluminum matrix by the liquid−solid reaction. The final nominal mass fraction of AlN_p in the composite was 12.3%. The density of the AlN_p/Al composite was calculated to be 2.68 g/cm^3 according to the Archimedes' Principle. What's more, to regulate the different spatial configurations of AlN_p and the heterogeneous microstructure, subsequent plastic deformation was carried out. The AlN_p/Al composite was extruded with an extrusion ratio of ~20 at 500 °C. According to our previous experiment tests, the extrusion ratio of 20 at 500 °C can obtain uniform and fine grains as well as improve the density and formability of the composite. To disperse the particles in the Al matrix, the extruded composites were subjected to hot rolling at 500 °C with an equivalent strain of approximately 0.7−1.4. The microstructures of the composite with equivalent strains of 0.7 and 1.4 are more representative according to our experiments with different equivalent strains. Deformation at this temperature can also improve the formability of the composite and reduce cracks. After hot rolling deformation, the morphology and spacing of the pure aluminum layer were also changed, then forming a lamellar heterostructured composite. Before each rolling pass, the sample was preheated at 500 °C for 5 min. The von Mises equivalent strain (ε_{VM}) after different rolling reductions can be calculated according to the following equation [26]:

$$\varepsilon_{\rm VM}=\frac{-2}{\sqrt{3}}\ln\frac{t}{t_0} \tag{1}$$

where t_0 and t are the plate thickness before and after rolling, respectively. The AlN_p/Al composite was firstly fabricated by a liquid−solid reaction method and then subsequent thermal-mechanical deformation treatments were carried out to regulate the microstructures. According to the obtained spatial configuration of AlN_p, three types of composites were referred to as Clustered-AlN_p/Al, Networked-AlN_p/Al and Uniformed-AlN_p/Al, respectively. The fabrication parameters of the three typical samples are displayed in Table 1.

2.2 Microstructure characterization

The microstructures of the AlN_p/Al composites were characterized using a field emission scanning electron microscope (FESEM, Quanta

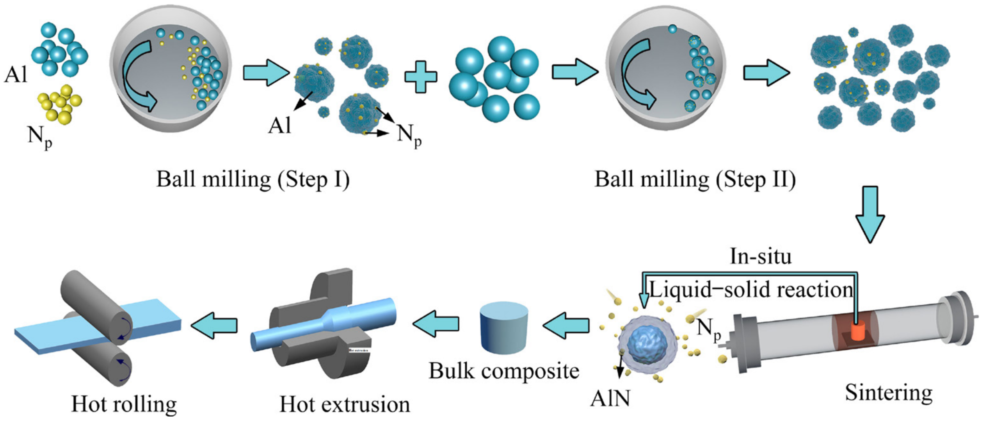

Fig. 1 Schematic diagram showing fabrication processes of heterostructured AlN_p/Al composites

Table 1 Fabrication parameters of three typical samples

Sample	Equivalent strain, ε_{VM}	Spatial configuration of particles
Clustered-AlN_p/Al	0	Cluster
Networked-AlN_p/Al	0.7	Network
Uniformed-AlN_p/Al	1.4	Uniform

250F, working at 20 kV), electron back-scattered diffraction (EBSD, Zeiss Auriga), transmission electron microscope (TEM, TECNAI 20, working at 200 kV) and high-resolution transmission electron microscopy (HRTEM, Titan G2 60−300, working at 300 kV). All the experiments were observed on the RD−ND (rolling direction−normal direction) plane of the sheets.

Specimens for SEM/EBSD characterization were prepared by mechanical polishing. The step size for EBSD scanning was 0.15 μm. Due to the limitation of angular precision, misorientations below 2° were excluded to avoid spurious boundaries. All EBSD data were analyzed using Channel 5 software. Thin foils for TEM observations were mechanically polished to the thickness of ~25 μm, and then polished by ion beam using Gatan 691 precision ion polishing system (PIPS).

2.3 Tensile test

A flat dog-bone tensile specimen with a gauge size of 5.5 mm × 3 mm × 2 mm was electro-discharge machined from the processed sheet. The tensile specimen axis was parallel to RD. The tensile tests were performed at room temperature using a universal tensile testing machine (LFM−20, Walter + baiag) at an initial strain rate of 3×10^{-3} s^{-1}. To make sure the accuracy of measurement, each sample was repeated at least three times.

3 Results

3.1 Microstructure features of AlN_p/Al composite

As shown in Figs. 2(a, b), the initial pure Al powder is spherical with an average particle size of ~2 μm, and the nitride plastid powder has a lamellar structure with a size of about 0.5 μm. After the ball-milling process, the size of the milled powder increases and the morphology is irregular (as shown in Fig. 2(c)). More details on the raw materials can be referred to in our previous work [27]. Figure 2(d) demonstrates the microstructure of the AlN_p/Al composite after sintering and the EDS point analysis of AlN_p. The inhomogeneous distribution of AlN_p can be observed, forming AlN_p-rich and AlN_p-poor domains. The EDS result shows the existence of Al and N elements in the composite and identifies the existence of the AlN_p phase.

Figure 3 shows the microstructures of three AlN_p/Al composites and the distribution characteristics of AlN_p on the longitudinal section. Figures 3(b, d, f) show the magnified images indicated

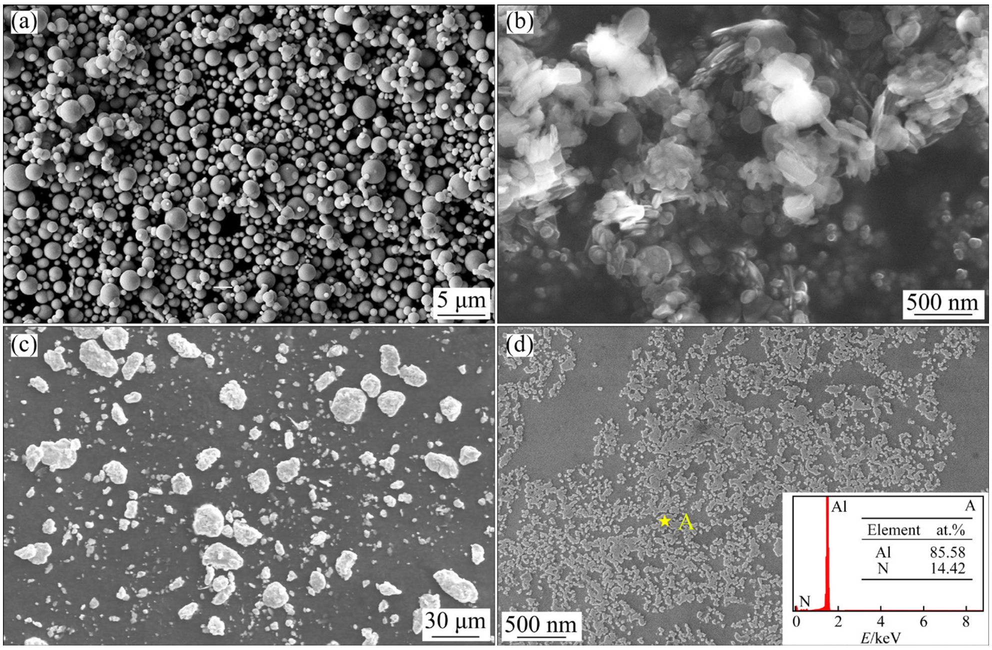

Fig. 2 Microstructures of raw materials and as-sintered AlN_p/Al composite: (a) Commercially pure Al powders; (b) Nitride plastid powders; (c) Milled powders; (d) As-sintered AlN_p/Al composite and EDS results of Point A

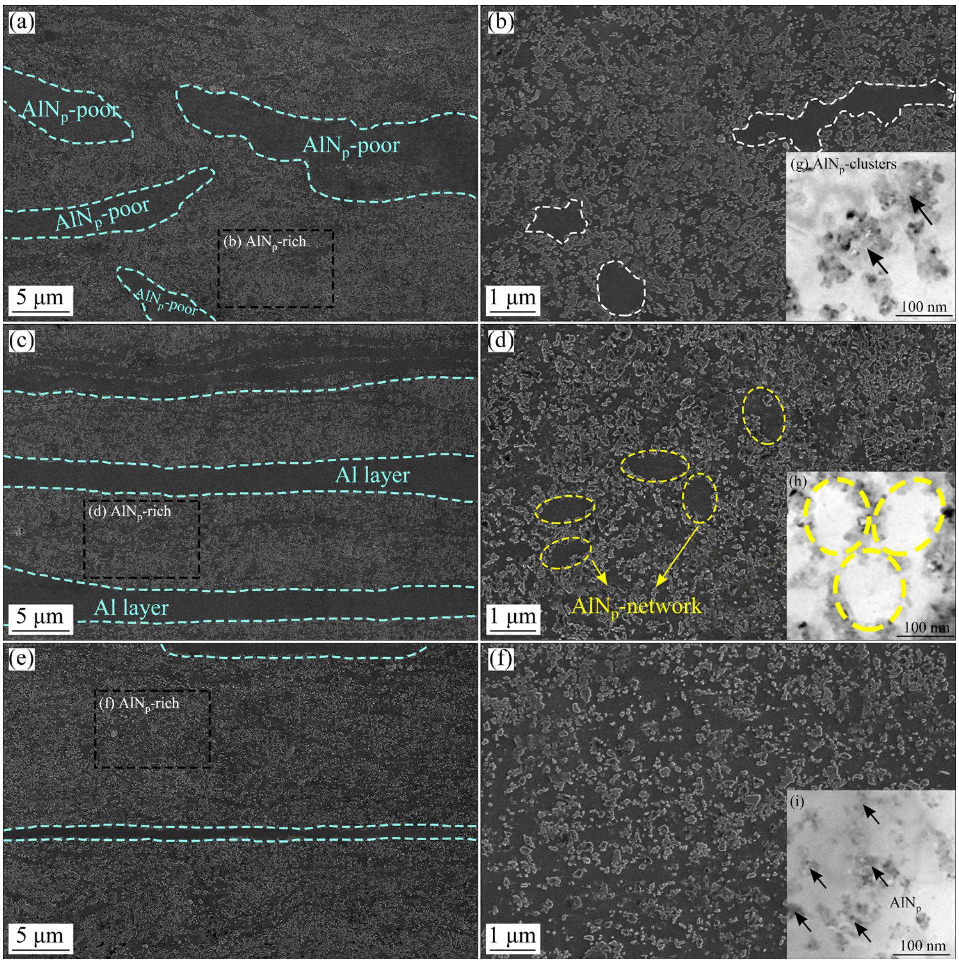

Fig. 3 Microstructure and particle spatial distributions in three AlN_p/Al samples: (a, b, g) Clustered-AlN_p/Al; (c, d, h) Networked-AlN_p/Al; (e, f, i) Uniformed-AlN_p/Al

by the black dotted boxes in Figs. 3(a, c, e), respectively. As shown in Figs. 3(a, b), the microstructure of the extruded sample includes two distinct zones, namely, the AlN_p-rich zone and the AlN_p-poor zone. In the AlN_p-rich zone, most of the particles are agglomerated together, while the pure aluminum lamella, i.e., AlN_p-poor zone (marked by green dotted lines), has an average wide space of approximately 6 μm. The extruded sample is thus referred to as Clustered-AlN_p/Al. To regulate the heterogeneous microstructure, the Clustered-AlN_p/Al composite was deformed by hot rolling with different equivalent strains (0.7 and 1.4). After rolling, it can be seen from Figs. 3(a, c, e) that the distribution of the AlN_p-rich zone in the matrix gradually changes from non-uniform distribution to lamellar distribution, the aluminum matrix layer is elongated along the rolling direction and the average width decreases to approximately 1.5 μm (Fig. 3(e)).

Moreover, according to the local magnified images of the AlN_p layer in Figs. 3(b, g), the average particle size of some large particle clusters is approximately 100 nm. In addition, there are several local areas with few particles (indicated by white dotted lines). When further deformation was applied, the AlN_p with an average particle size of approximately 65 nm in the matrix shows a continuous or semi-continuous network structure, as indicated by the yellow dotted line in Figs. 3(c, d, h), which was also confirmed in our previous work that the distribution of AlN_p presented network under a certain deformation (referred to as Networked-AlN_p/Al) [28]. When the applied equivalent strain increased to 1.4, most AlN_p networks are destroyed and AlN_p particles with an average size of approximately 50 nm are uniformly dispersed in the matrix, as shown in Figs. 3(f, i). Thus, this sample is referred to as Uniformed-AlN_p/Al.

3.2 Matrix grain structure of AlN_p/Al composite

To study the influence of particle distribution on aluminum matrix grains during deformation, EBSD analysis was carried out. Figure 4 shows the crystal orientation maps and Al grain size distributions in the three AlN_p/Al composites. The black lines in Figs. 4(a−c) represent grain boundaries with misorientation angles above 15° (high angle grain boundaries, $\theta \geq 15°$). As shown in Fig. 4(a), both elongated coarse grains and fine equiaxed grains can be seen in the Al matrix of the Clustered-AlN_p/Al composite. The average width of the coarse grains in the AlN_p-poor zone is approximately 2.5 μm, which have been elongated along the extrusion direction. It is noticed that most fine equiaxed grains are distributed in the AlN_p-rich zone. In fact, the AlN_p-poor zones are recognized as the soft zones and the AlN_p-rich zones are recognized as the hard zones. After the rolling deformation, it can be seen that a lamellar heterogeneous structure with an alternative soft zone (marked as black dotted lines) and hard zone is formed in the Networked-AlN_p/Al composite (Fig. 4(b)). The average grain size of elongated coarse grains in the soft zones is reduced to less than 8 μm in length and less than 2 μm in width. Meanwhile, the average grain size in the hard zones with relatively dispersed AlN_p also decreases. With the further increase of the applied equivalent strain to 1.4, the AlN_p particles with sizes of ~60 nm tend to be uniformly distributed and more fine grains are formed in the matrix for Uniformed-AlN_p/Al composite, as seen in Fig. 4(c). In addition, the grain size distributions of the three samples are shown in Figs. 4(d−f). It can be seen that the average grain size is reduced from 1.58 to 1.18 and 0.86 μm.

It is known that the geometrically necessary dislocations (GNDs) will accumulate in grains or interfaces with a strong strain gradient during the rolling process [15,29]. The GND density (ρ_{GND}) can be calculated according to the strain gradient model proposed by GAO et al [30] and the equation provided by KUBIN and MORTENSEN [31]:

$$\rho_{GND}=\alpha\theta/(bx) \tag{2}$$

where b is the magnitude of the Burgers vector, x is the unit length, α is a constant equal to 2, and the misorientation angle (θ) is the kernel average misorientation (KAM), which is the average misorientation angle of a measurement point. Thus, the GND densities in the soft and hard domains of

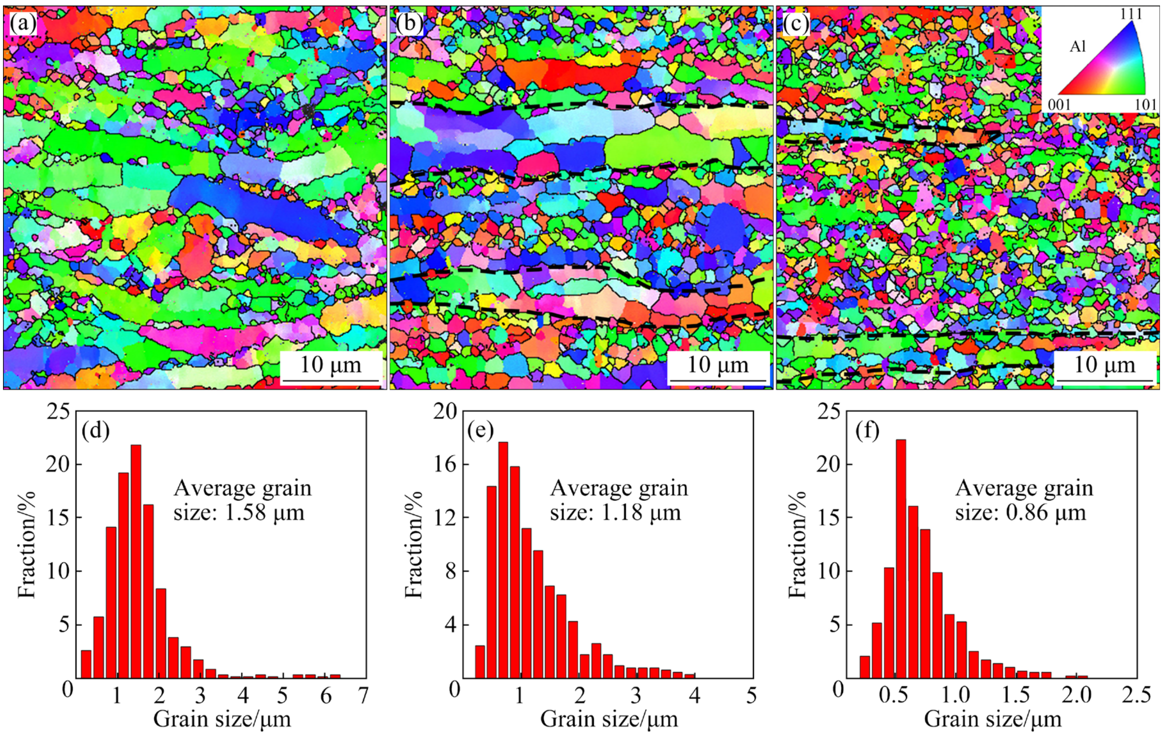

Fig. 4 EBSD analysis results (a−c) of α(Al) grains and corresponding grain size distributions (d−f) in three AlN_p/Al composites: (a, d) Clustered-AlN_p/Al; (b, e) Networked-AlN_p/Al; (c, f) Uniformed-AlN_p/Al (The inset in Fig. 4(c) is the inverse pole figure color code)

the AlN_p/Al composites were calculated according to the EBSD results. The results are shown in Fig. 5(a), where the different colors represent the variation in the intensity of GND density, i.e., the red represents higher values of GND density and the blue is associated with lower values. Obviously, the GND distribution in the matrix of the Clustered-AlN_p/Al and Networked-AlN_p/Al composites is inhomogeneous, suggesting that strain localization occurs at the interfaces between hard zones and soft zones. However, after the hot rolling process, the GND distribution in the α(Al) matrix of the Uniformed-AlN_p/Al composites is relatively uniform, as shown in Fig. 5(c), demonstrating that the strain distribution becomes more homogeneous in the matrix. Specifically, the quantitative results are shown in Figs. 5(d−f), respectively. The GND density for the Uniformed-AlN_p/Al is 7.92×10^{15} m^{-2}, which is much higher than that of the Clustered-AlN_p/Al (6.01×10^{15} m^{-2}) and the Networked-AlN_p/Al (6.39×10^{15} m^{-2}) composites. Meanwhile, the increased GNDs in the matrix will be also helpful for the enhanced mechanical properties.

The grain structure and the AlN_p distribution in the Clustered-AlN_p/Al sample are further revealed by the TEM images, as shown in Fig. 6. Both the AlN_p-rich zone and AlN_p-poor zone can be seen in Fig. 6(a). The α(Al) matrix grains (marked as yellow dotted lines) are elongated along the extrusion direction in AlN_p-poor zone. However, the Al grains

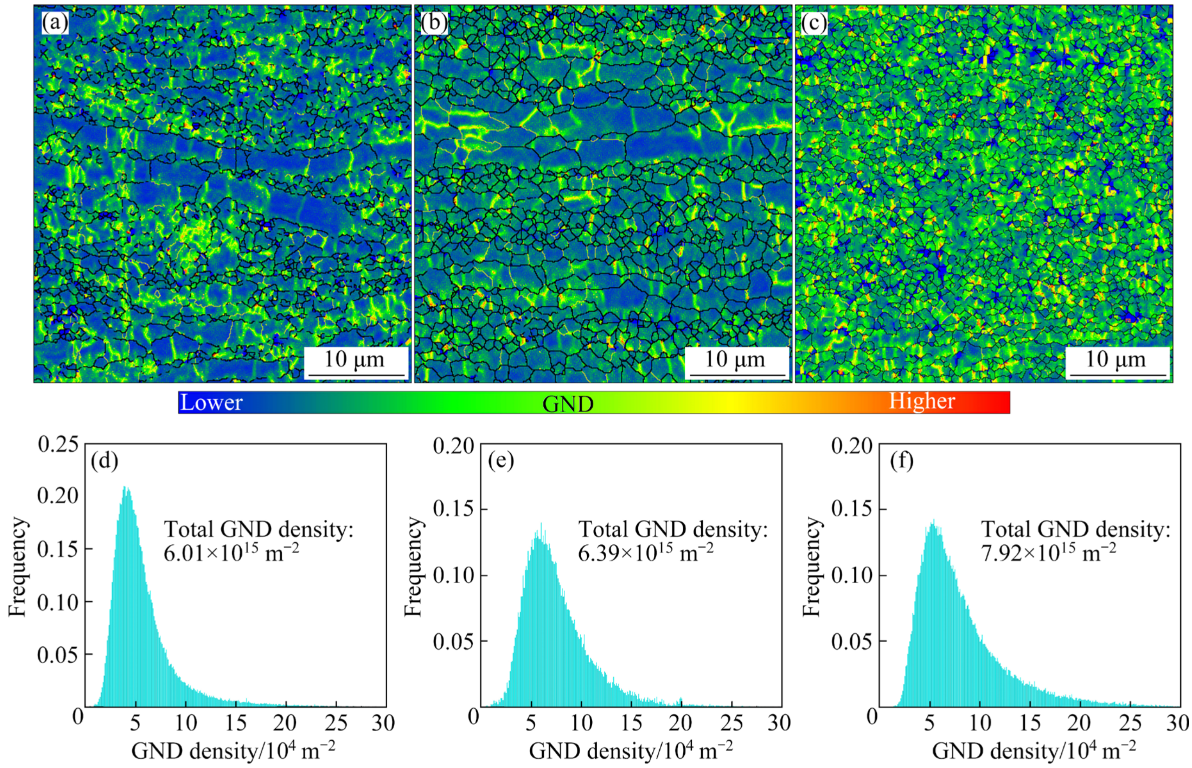

Fig. 5 GND density mapping for three samples: (a, d) Clustered-AlN_p/Al; (b, e) Networked-AlN_p/Al; (c, f) Uniformed-AlN_p/Al

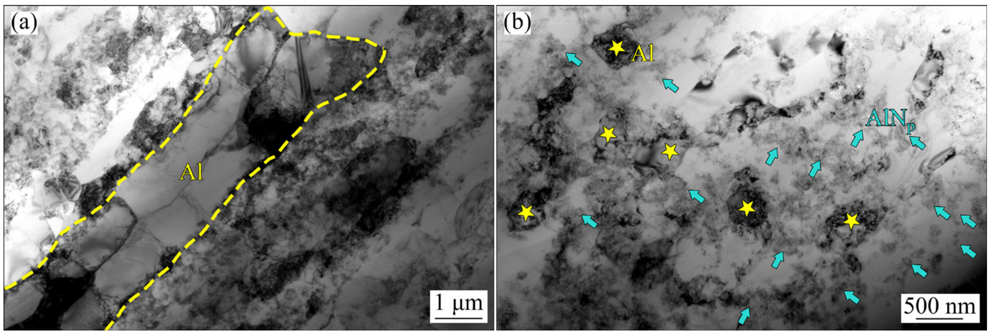

Fig. 6 TEM images showing microstructure of Clustered-AlN_p/Al sample (a) and AlN_p distribution in particle-rich zone (b)

are refined to an ultrafine structure in the AlN_p-rich zone (marked by blue arrows in Fig. 6(b)), due to the strong pinning effect of the AlN_p on the dislocations and grain boundaries during the hot deformation process [32,33]. These results are consistent with the above EBSD analysis.

3.3 Interface characteristics of Uniformed-AlN_p/Al composite

Figure 7 shows the HRTEM analysis results for the Uniformed-AlN_p/Al composite. According to the HAADF-STEM image (Fig. 7(a)), it can be seen that some dark particles are dispersed in the gray Al matrix, the matrix grain has an ultrafine structure, and most grain sizes are smaller than 0.5 μm. The dark particles are the in situ formed AlN_p proved by the EDS mapping analysis. The interface structure between AlN and the matrix was further investigated. The HRTEM images and the corresponding fast Fourier transformation (FFT) image are shown in Figs. 7(d−f). From the FFT image (Fig. 7(f)), the AlN_p crystal is oriented to the $[01\bar{1}0]$ zone axis, and the α(Al) crystal is oriented to the [011] zone axis. Furthermore, it is found that the (0002) crystal plane of AlN_p is parallel to the $(\bar{2}00)$ crystal plane of α(Al), and the two phases are semi-coherently bonded at the interface, indicating a robust bonding between AlN_p and the α(Al) matrix. It is considered that this good atomic bonding plays an important role in strength enhancement.

3.4 Tensile properties of AlN_p/Al composites

Figures 8(a, b) show the stress−strain curves at room temperature of the AlN_p/Al composites with different thermal-mechanical treatments. The corresponding strength and elongation are shown in Fig. 8(c) and the detailed values are given in Table 2. The yield strength (YS) and ultimate tensile strength (UTS) of the Clustered-AlN_p/Al composite are ~279.6 and ~334.5 MPa, and the corresponding uniform elongation (ε_{ue}) and the elongation to failure (ε_{ef}) are ~4.2% and ~6.8%, respectively. After the thermal-mechanical deformation treatment, the strength and ductility of the Networked-AlN_p/Al composite and Uniformed-

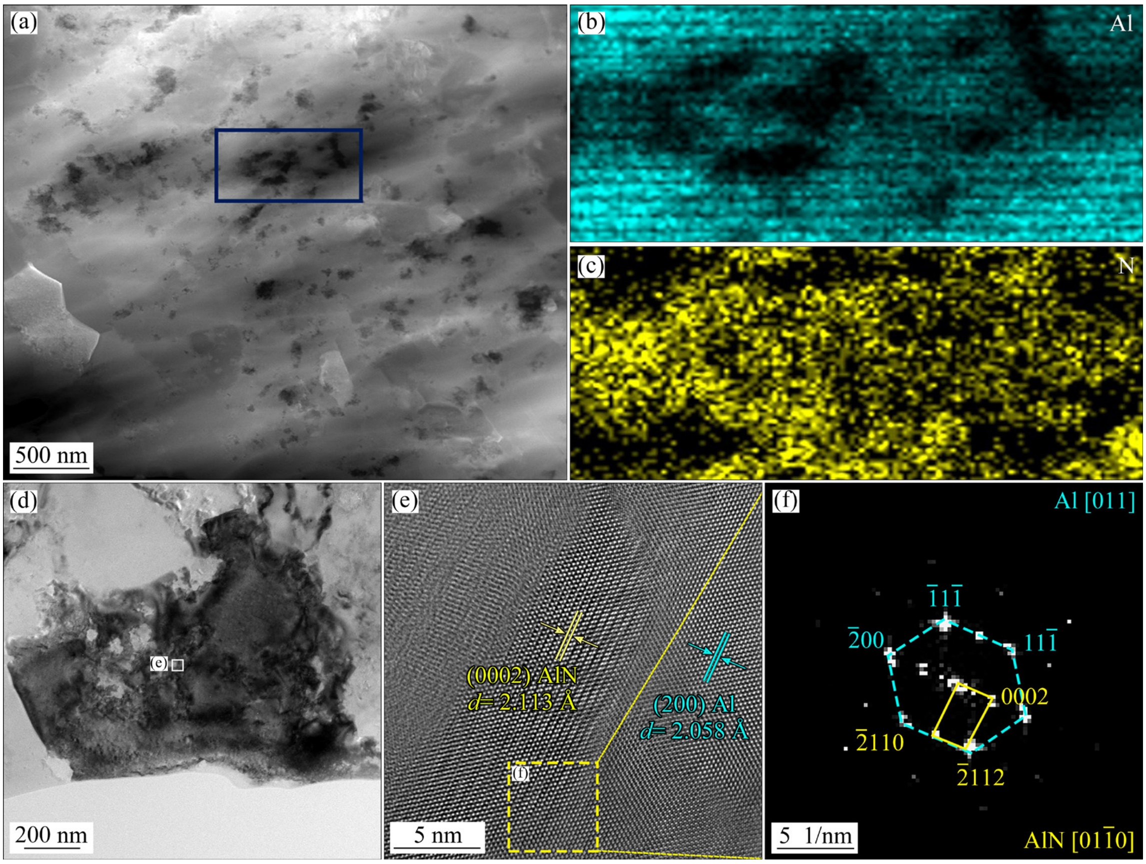

Fig. 7 HRTEM analysis results for Uniformed-AlN_p/Al sample: (a−c) HAADF-STEM image and EDS mappings of Al and N elements in matrix; (d) α(Al) grain containing AlN_p; (e) HRTEM image of interface between AlN_p and α(Al); (f) Corresponding FFT image of dashed rectangle region in (e)

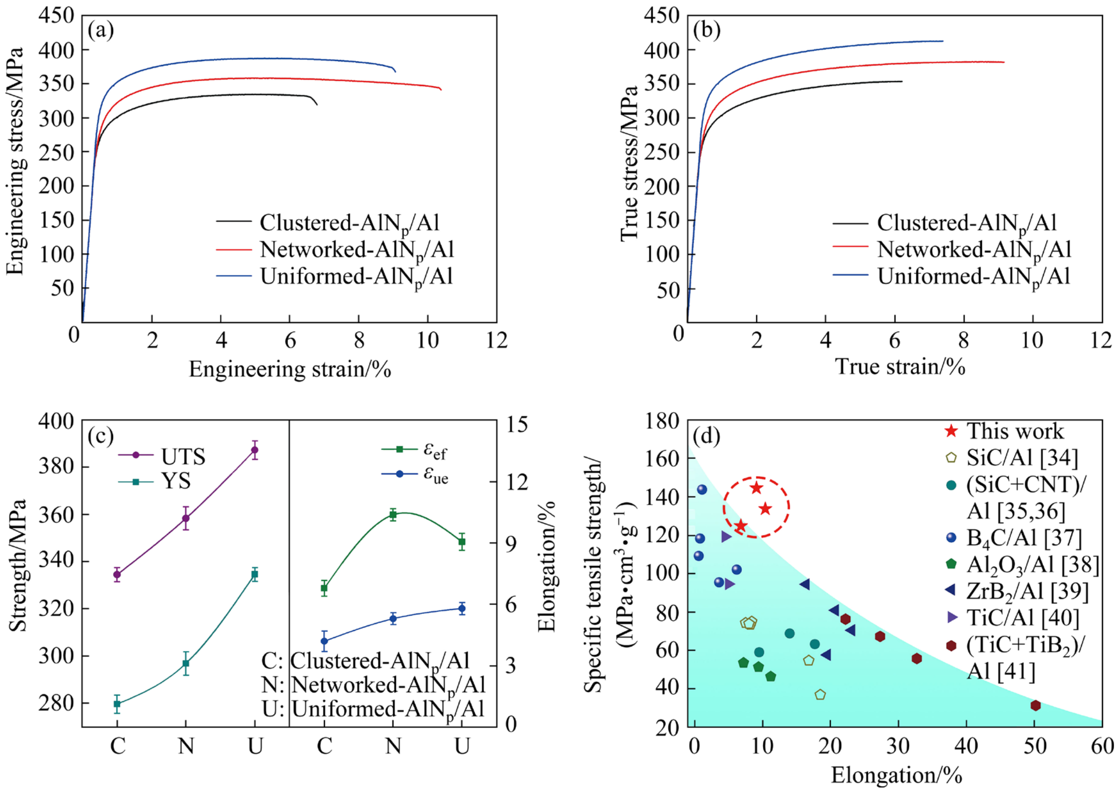

Fig. 8 Tensile properties of AlN$_p$/Al composites: (a) Engineering stress−strain curves; (b) True stress−strain curves; (c) Strength and elongation of different AlN$_p$/Al samples; (d) Comparisons of specific tensile strength and elongation of AlN$_p$/Al composites in this work and other PRAMCs [34−41]

Table 2 Mechanical properties of AlN$_p$/Al composites at RT

Sample	YS/MPa	UTS/MPa	ε_{ue}/%	ε_{ef}/%	PSE/(MPa·%)	STS/(MPa·cm^3·g^{-1})
Clustered-AlN$_p$/Al	279.6±4	334.5±3	4.2±0.5	6.8±0.4	~2274.6	~124.8
Networked-AlN$_p$/Al	296.8±5	358.4±5	5.3±0.3	10.4±0.3	~3727.4	~133.7
Uniformed-AlN$_p$/Al	334.6±3	387.4±4	5.8±0.3	9.1±0.4	~3525.4	~144.6

AlN$_p$/Al composite are gradually increased. The YS is increased to ~296.8 and ~334.6 MPa and the UTS is enhanced to ~358.4 and ~387.4 MPa, respectively. Meanwhile, the ε_{ue} is increased to 5.3% and 5.8%, respectively. The ε_{ef} is increased to 10.4% and 9.1%, respectively. It can be seen that a simultaneous increase of strength and ductility has been achieved without the sacrifice of ductility. The product of strength and elongation (PSE) of the composite, which can be used to estimate the toughness of the materials, was also calculated, as shown in Table 2. It can be seen that the PSE of the Networked-AlN$_p$/Al composite and Uniformed-AlN$_p$/Al composite are around 3727.4 and 3525.4 MPa·%, respectively, ~64% and ~55% higher than that of Clustered-AlN$_p$/Al composite, respectively. Therefore, it is indicated that the lamellar heterostructured composites exhibit an excellent combination of strength and ductility. Furthermore, the specific tensile strength (STS) values of the Networked-AlN$_p$/Al and Uniformed-AlN$_p$/Al composites are calculated to be about 133.7 and 144.6 MPa·cm^3/g. Figure 8(d) compares the STS and elongation of the AlN$_p$/Al composites in this work and other PRAMCs [34−41]. It can be seen that the AlN$_p$/Al composites exhibit much better STS−elongation synergy than other PRAMCs. Therefore, the AlN$_p$/Al composites with heterogeneous matrix grain structure and relatively dispersive particle characteristics exhibit an outstanding balance of specific tensile strength and elongation.

4 Discussion

4.1 Evolution of particle configuration

It is shown that the network structure of AlN_p can be formed during the in-situ reaction process of Al powders and the nitrogen plasmids. However, the amount of AlN_p networks in the extruded sample is small due to the large volume fraction of AlN_p. Then, the large AlN_p clusters are distributed in the matrix, as shown in Fig. 3(g), which is not beneficial to the mechanical property. Therefore, hot rolling deformation is used to regulate the spatial distribution of particles. During plastic deformation, the shear force was applied to the matrix of the composite, leading to the shear flow of the aluminum matrix [42−44]. Consequently, the large AlN_p clusters were dispersed in the AlN_p-rich zone by the shear flow stress. At the same time, small AlN_p networks were further expanded to form nano and micron-scale network structures, as shown in Figs. 3(d, h). With further deformation, the network structure of AlN_p was dispersed more significantly and the particles were uniformly distributed (shown in Fig. 3(f)). Accordingly, hot rolling deformation treatment has a significant effect on the spatial configuration of particles.

Generally, the homogenization distribution of the particles in the matrix depends on the sizes of the constituents and the processing method. TAN and ZHANG [43], and SABIROV et al [44] have proposed a geometrical model to predict the critical size condition of a uniform distribution of particles after different deformation processes (including extrusion and hot rolling):

$$d_{\mathrm{p}} \geq \frac{d_{\mathrm{m}}}{\left[\left(\dfrac{\pi}{\sigma f}\right)^{1/3}-1\right]\dfrac{\sqrt{R}}{1-R'}} \tag{3}$$

where d_p is the critical particle size, d_m is the average grain size of the composite, f is the particle volume fraction, R is the extrusion ratio (during extrusion) and R' is the reduction ratio (during rolling). It can be seen that the critical value (d_p) is related to the d_m, f and the strains induced into the sample during deformation. The uniform distribution of particles can be realized when the particle size is not less than d_p. The parameters calculated by Eq. (3) are given in Table 3. According to these data, the particle size of the Clustered-AlN_p/Al composite is smaller than the d_p value of 168.3 nm, and the aggregation can occur (Fig. 3(g)). The value of d_p is 69.2 nm in the Networked-AlN_p/Al composite, which is slightly larger than the particle size. Some large particle clusters were broken but did not form a uniform distribution. For the Uniformed-AlN_p/Al composite, the value of d_p decreases to 27.5 nm, which is less than the size of the AlN_p, indicating that a homogeneous particle distribution can be obtained. And there is a good agreement between the calculated values and experimental results (as shown in Figs. 3(g−i)). Therefore, we can obtain three kinds of composites characterized by different microstructures after deformation treatment.

Table 3 Average grain size (d_m), critical particle size (d_p) and actual particle size (D_p) of AlN_p/Al composites in this work

Sample	d_m/μm	d_p/nm	D_p/nm
Clustered-AlN_p/Al	1.58	168.3	100
Networked-AlN_p/Al	1.18	69.2	65
Uniformed-AlN_p/Al	0.86	27.5	50

4.2 Strengthening mechanisms

As mentioned above (Fig. 8), both the Networked-AlN_p/Al and Uniformed-AlN_p/Al composites behave much better in strength and ductility synergy than the Clustered-AlN_p/Al composite. The strengthening mechanisms should be mainly attributed to grain refinement strengthening and hetero-deformation induced (HDI) stress strengthening [17]. According to the well-known Hall−Petch relationship, the yield stress σ_y is related to the grain size by [45]

$$\sigma_{\mathrm{y}}=\sigma_0+kD^{-1/2} \tag{4}$$

where σ_y is the yield stress, σ_0 is the friction stress, k is a constant that reflects the boundary resistance to dislocation slip, and D is the mean grain size of the matrix. The yield strength can be increased with the reduction of grain size. According to statistics in Figs. 4(d−f), after thermal-mechanical treatment, grain sizes of Networked-AlN_p/Al and Uniformed-AlN_p/Al composites decreased to ~1.18 and ~0.86 μm, respectively. Therefore, massive grain boundaries were generated in the composites, which hindered the dislocation movement and led to an increase of yield strength.

Among three composites, the Uniformed-AlN_p/Al composite has optimal YS, UTS, and ductility combinations. To investigate the distribution of accumulated dislocations in the Uniformed-AlN_p/Al composite during the tensile deformation process, the TEM analysis was performed before and after tensile deformation. Before the tensile deformation, the AlN_p (indicated by the green arrows) are distributed in grains and at grain boundaries (Fig. 9(a)). Some tangled dislocations (indicated by the blue arrows) accumulate in α(Al) grains due to the pinning effect of the AlN_p. However, almost no dislocations are seen in the domain without particles, as shown in Fig. 9(a). The Uniformed-AlN_p/Al composite consists of soft and hard domains, and the soft domain is constrained by the hard ones. During tensile deformation, GNDs are generated in micron-size grains (the soft zones) to accommodate the local plastic strain gradients between the hard and soft domains, as shown in Figs. 9(b, c).

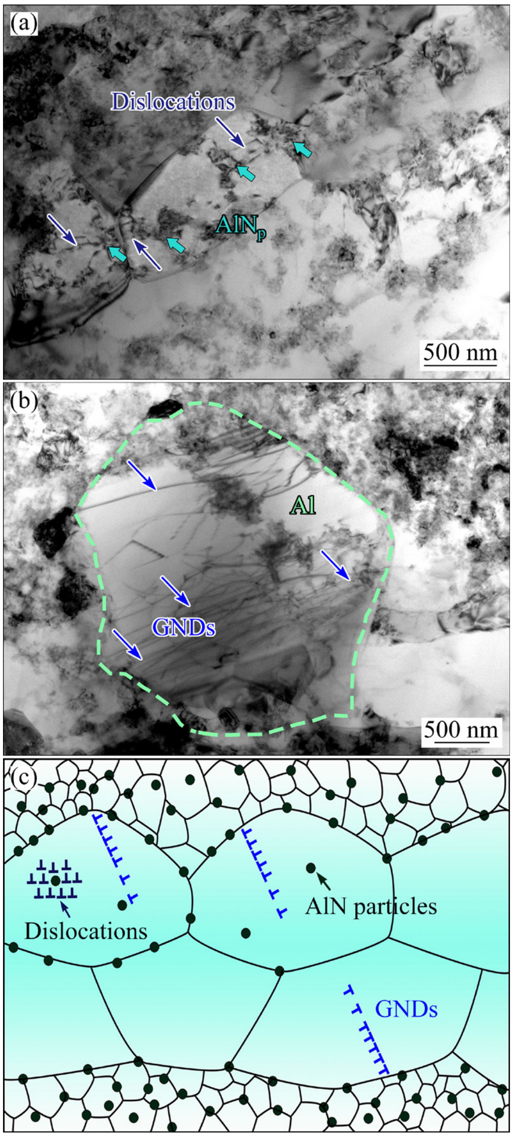

Fig. 9 TEM images of Uniformed-AlN_p/Al sample before and after tensile test: (a) Amounts of accumulated dislocations before tensile test; (b) Accumulation of GNDs after tensile test; (c) Schematic diagram showing dislocations and GNDs of composites after tensile test

To quantitatively estimate the contribution of the HDI hardening, the cyclic load−unload−reload (LUR) tensile tests were performed. Figure 10(a) shows the LUR curves of AlN_p/Al composites. And the HDI stress (σ_{HDI}) under different strains can be calculated by the following equation [46]:

$$\sigma_{HDI} = \frac{\sigma_r + \sigma_u}{2} \tag{5}$$

where σ_r and σ_u are the reloading yield stress and unloading yield stress, as indicated in Fig. 10(b).

As shown in Fig. 10(c), the HDI stress of different composites increases with the applied strain, promoting high strain hardening. However, the HDI stress of Uniformed-AlN_p/Al composite is significantly higher than that of the other two samples, indicating that HDI stress plays a particularly significant role in this sample. Figure 10(d) presents the area of the hysteresis loops obtained from the LUR tensile tests. The area of the loops increases with strain and the Uniformed-AlN_p/Al composite presents a larger hysteresis, indicating a stronger Bauschinger effect, which is consistent with the assessment by the HDI stress, as shown in Fig. 10(c).

Figure 11 shows the volume fraction and average grain size of soft and hard zones in different composites. It can be seen that the volume fraction of the soft zones is approximately 21% in the heterostructured Uniformed-AlN_p/Al composite (Fig. 11(a)). In this structure, the interface affected zone of the hard and soft phase is maximized, which increases the density of GNDs and results in higher strain hardening [47,48]. The increase of HDI hardening is mainly due to the increase of non-uniform interface, including the AlN_p/Al interface and matrix grain interface. As shown in Fig. 11(b), the average grain sizes in both soft and hard zones are gradually refined with the increase of the applied equivalent strain.

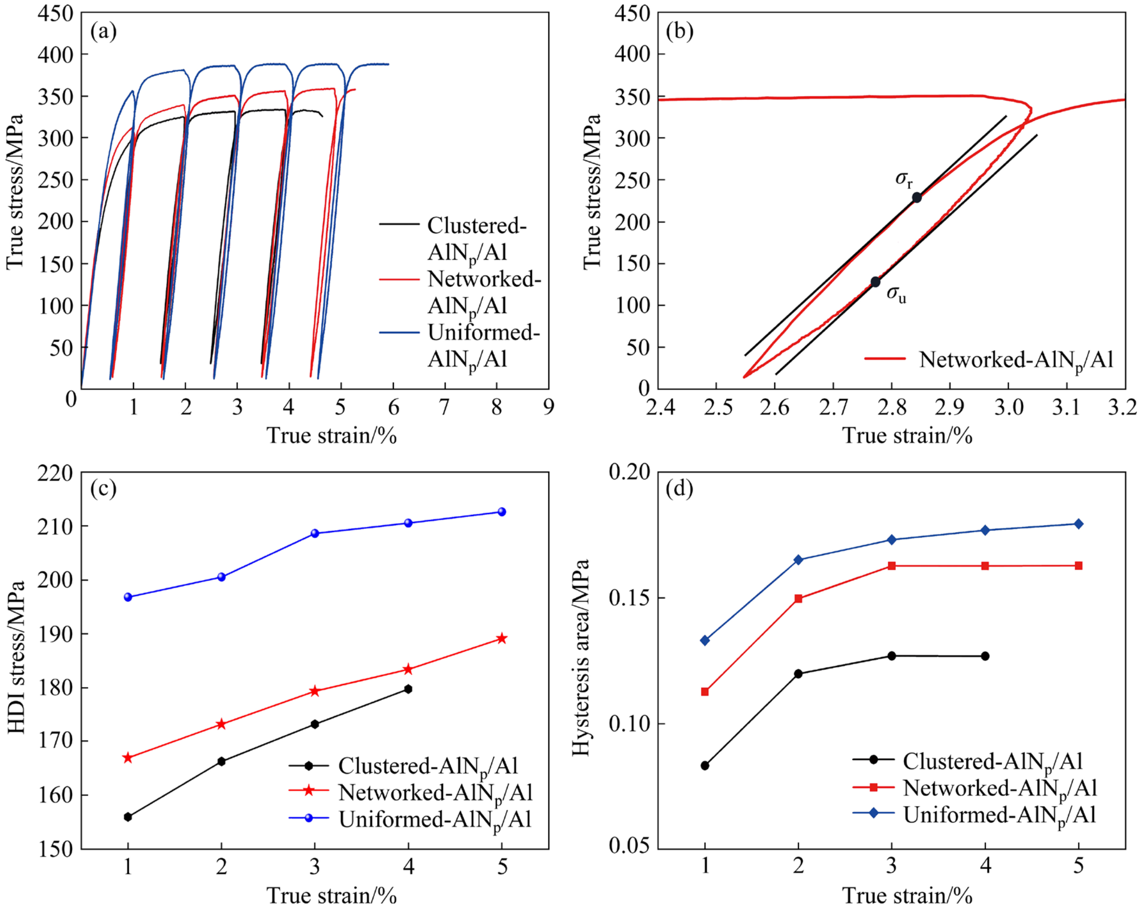

Fig. 10 LUR tensile test results: (a) LUR curves of three AlN_p/Al composites; (b) Schematic of hysteresis loops with σ_u and σ_r defined at 3% true strain of Networked-AlN_p/Al composite; (c) HDI stress versus applied strain curves in three AlN_p/Al composites; (d) Area of hysteresis loops varying with true strain in three AlN_p/Al composites

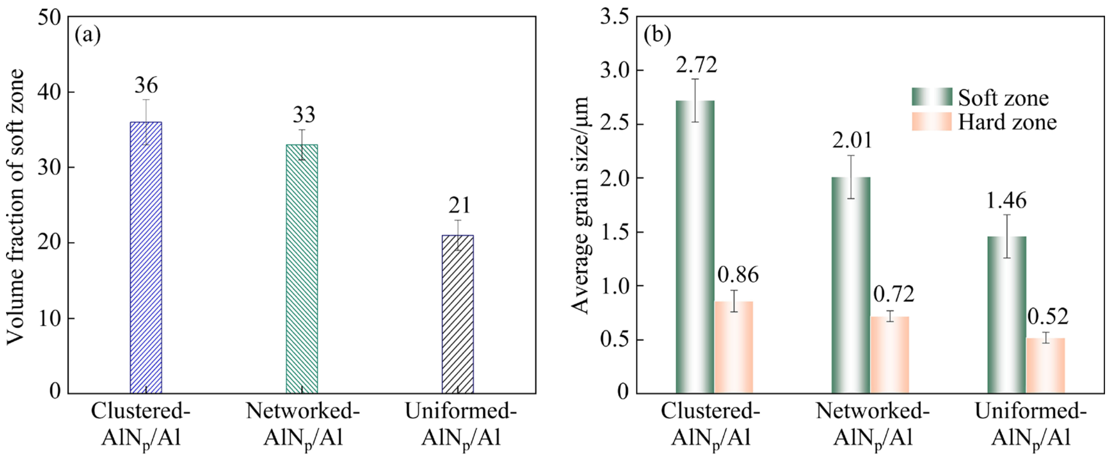

Fig. 11 Volume fraction of soft zone (a) and average grain size of soft and hard zones (b) in different composites

4.3 Fracture behavior

To provide insight into mechanical behavior and establish a relationship between microstructures and mechanical properties, the fracture surface morphologies were investigated, as shown in Fig. 12. Numerous dimples can be seen on the entire fracture surfaces, indicating that all the composites are fractured via the ductile mechanism. As shown in Figs. 12(a, b), the dimples of the Clustered-AlN_p/Al composite are not uniformly distributed, which is mainly related to the distribution configuration of AlN_p in the composite.

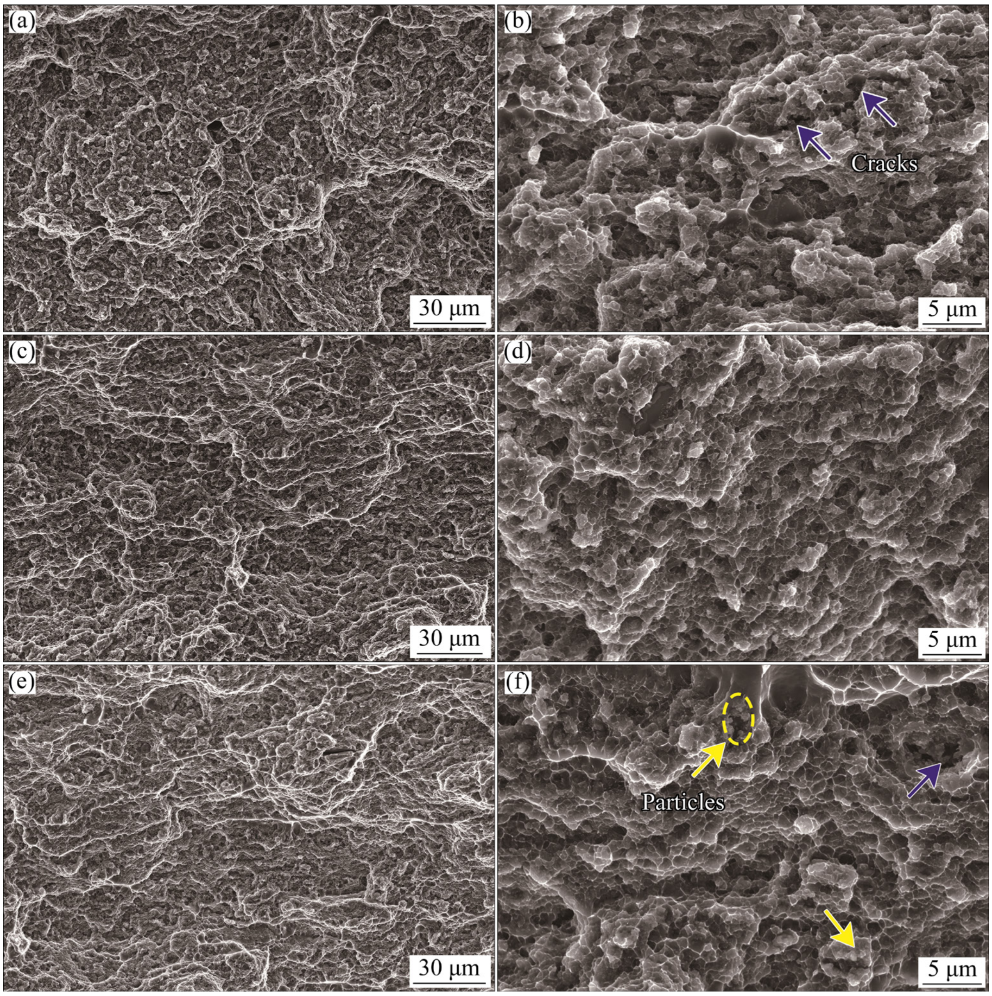

Fig. 12 Tensile fracture morphologies of three composites: (a, b) Clustered-AlN_p/Al; (c, d) Networked-AlN_p/Al; (e, f) Uniformed-AlN_p/Al

Some big dimples with sharp edges and the exposed AlN_p are seen in the center of the dimples. And there are some cracks (marked by blue arrows) in Fig. 12(b). As displayed in Figs. 12(c, d), the dimples are smaller, the tear edges are smooth and no obvious cracks are observed on the fracture surface. On the fracture surface of the Uniformed-AlN_p/Al composite, the dimples are uneven and some dimples are nearly 5 μm with few exposed AlN_p. The cracks nucleate at the particle agglomerates marked by yellow arrows in Fig. 12(f). The increased elongation to failure for the Networked-AlN_p/Al is mainly attributed to the robust bonding of AlN_p and Al interface and the network structure of AlN_p. During the tensile deformation process, the network structure can deflect the cracks, reduce the stress concentration on the crack tip, and effectively hinder crack propagation [49] in the AlN_p-rich zones. NIE et al [50] studied the high temperature performance of AlN_p/Al composites with a network structure and showed that the network structure can effectively hinder crack propagation and improve the ductility of the materials. As the deformation increases, the homogeneous distribution of particles helps to suppress strain localization in the process of tensile deformation [51], which contributes to the improvement of ductility.

5 Conclusions

(1) The configuration of AlN_p in the matrix has been regulated from agglomerated cluster to a network structure, and then a relatively more uniform particle distribution has been achieved after the thermal-mechanical treatment. The α(Al) matrix grains both in the particle-rich zone and particle-poor zone are refined, and the final average grain size decreases from 1.58 to 1.18 and to

0.86 μm.

(2) The yield strength and ultimate tensile strength of the Uniformed-AlN_p/Al composite are ~334.6 and ~387.4 MPa, respectively, which increases by ~55 and ~52.9 MPa compared with those of the Clustered-AlN_p/Al composite. Meanwhile, the elongation to failure is also increased from 6.8% to 9.1%, achieving an excellent synergy of strength and ductility. The lamellar heterostructured composites exhibit an outstanding balance of specific tensile strength and elongation, which is much superior to the reported aluminum matrix composite.

(3) It is shown that the HDI stress and HDI hardening effect of the Uniformed-AlN_p/Al composite are significantly enhanced and are superior to those of the other two samples. The main strengthening mechanisms for the hetero-structured AlN_p/Al composite are fine grain strengthening and HDI hardening.

CRediT authorship contribution statement

Yu-yao CHEN: Investigation, Methodology, writing – Origin draft, Writing − Review & editing; **Jin-feng NIE:** Investigation, Conceptualization, Funding acquisition, Supervision, Writing – Review & editing; **Yong FAN:** Investigation; **Lei GU:** Data curation; **Ke-wei XIE:** Data analysis; **Xiang-fa LIU:** Supervision, Writing – Review & editing; **Yong-hao ZHAO:** Supervision, Writing – Review & editing.

Declaration of competing interest

The authors declare that they have no known competing financial interests or personal relationships that could have appeared to influence the work reported in this paper.

Acknowledgments

This work is supported by the Key Program of National Natural Science Foundation of China (No. 51931003), the National Natural Science Foundation of China (Nos. 52271033, 52071179), the Natural Science Foundation of Jiangsu Province, China (No. BK20221493), and the Foundation of Qinglan Project for Colleges and Universities in Jiangsu Province, China.

References

[1] ZHANG Zhi-ming, FAN Gen-lian, TAN Zhan-qiu, ZHAO Hai-tao, XU Yan-jin, XIONG Ding-bang, LI Zhi-qiang. Towards the strength−ductility synergy of Al_2O_3/Al composite through the design of roughened interface [J]. Composites Part B: Engineering, 2021, 224: 109251.

[2] LUO Si-wei, WU Yue, CHEN Biao, SONG Min, YI Jian-hong, GUO Bai-song, WANG Qi-wei, YANG Yong, LI Wei, YU Zhen-tao. Effects of Cu content on microstructures and compressive mechanical properties of CNTs/Al−Cu composites [J]. Transactions of Nonferrous Metals Society of China, 2022, 32(12): 3860−3872.

[3] NIE Jin-feng, CHEN Yu-yao, CHEN Xiang, LIU Xiang-fa, LIU Gui-liang, ZHAO Yong-hao, ZHU Yun-tian. Stiff, strong and ductile heterostructured aluminum composites reinforced with oriented nanoplatelets [J]. Scripta Materialia, 2020, 189: 140−144.

[4] WOLF W, E SILVA L P M, ZEPON G, KIMINAMI C S, BOLFARINI C, BOTTA W J. Single step fabrication by spray forming of large volume Al-based composites reinforced with quasicrystals [J]. Scripta Materialia, 2020, 181: 86−91.

[5] XIE Ke-wei, NIE Jin-feng, HU Kai-qi, MA Xia, LIU Xiang-fa. Improvement of high-temperature strength of 6061 Al matrix composite reinforced by dual-phased nano-AlN and submicron-Al_2O_3 particles [J]. Transactions of Nonferrous Metals Society of China, 2022, 32(10): 3197−3211.

[6] GENG Run, ZHAO Qing-long, QIU Feng, JIANG Qi-chuan. Simultaneously increased strength and ductility via the hierarchically heterogeneous structure of Al−Mg−Si alloys/ nanocomposite [J]. Materials Research Letters, 2020, 8(6): 225−231.

[7] XIAO Hong-yu, LI Yu-gang, GENG Ji-wei, LI Hong-ping, WANG Ming-liang, CHEN Dong, LI Zhu-guo, WANG Hao-wei. Effects of nano-sized TiB_2 particles and Al_3Zr dispersoids on microstructure and mechanical properties of Al−Zn−Mg−Cu based materials [J]. Transactions of Nonferrous Metals Society of China, 2021, 31(8): 2189−2207.

[8] TOOZANDEHJANI M, OSTOVAN F, JAMALUDIN K R, AMRIN A, MATORI K A, SHAFIEI E. Process−microstructure−properties relationship in Al−CNTs−Al_2O_3 nanocomposites manufactured by hybrid powder metallurgy and microwave sintering process [J]. Transactions of Nonferrous Metals Society of China, 2020, 30(9): 2339−2354.

[9] SUN Xin-da, HAO Xiao-jie, NIE Jin-feng, FAN Yong, CHEN Yu-yao, LIU Si-da, LIU Xiang-fa, ZHAO Yong-hao. Microstructure and enhanced cryogenic tensile property of a heterostructured Al−AlN/Al−Mg composite fabricated by accumulative roll bonding (ARB) [J]. Journal of Materials Research and Technology, 2022, 21: 532−545.

[10] CHEN Gang, WAN Jia, HE Ning, ZHANG Hong-ming, HAN Fei, ZHANG Yu-min. Strengthening mechanisms based on reinforcement distribution uniformity for particle reinforced aluminum matrix composites [J]. Transactions of Nonferrous Metals Society of China, 2018, 28(12): 2395−2400.

[11] LI Shun, XIONG De-gan, LIU Meng, BAI Shu-xin, ZHAO Xun. Thermophysical properties of SiC/Al composites with three dimensional interpenetrating network structure [J]. Ceramics International, 2014, 40(5): 7539−7544.

[12] YANG Hua-bing, GAO Tong, LIU Gui-liang, ZHAO Xiao-jun, CHEN Hou-wen, WANG Hai-chao, NIE Jin-feng, LIU Xiang-fa. Simultaneously improving strength and ductility for Al−Cu−Mg alloy via threadiness array of TiC nanoparticles [J]. Materialia, 2019, 6: 100333.

[13] ROY S, GIBMEIER J, KOSTOV V, WEIDENMANN K A, NAGEL A, WANNER A. Internal load transfer in a metal matrix composite with a three-dimensional interpenetrating structure [J]. Acta Materialia, 2011, 59: 1424−1435.

[14] SCHERM F, VÖLKL R, NEUBRAND A, BOSBACH F, GLATZEL U. Mechanical characterisation of interpenetrating network metal−ceramic composites [J]. Materials Science and Engineering A, 2010, 527: 1260−1265.

[15] MIRACLE D B, PANDEY A B, MAJUMDAR B S. Laminated particulate-reinforced aluminum composites with improved toughness [J]. Acta Materialia, 2001, 49: 405−417.

[16] WU Xiao-lei, ZHU Yun-tian. Heterogeneous materials: A new class of materials with unprecedented mechanical properties [J]. Materials Research Letters, 2017, 5(8): 527−532.

[17] ZHU Yun-tian, WU Xiao-lei. Perspective on hetero-deformation induced (HDI) hardening and back stress [J]. Materials Research Letters, 2019, 7(10): 393−398.

[18] WU Xiao-lei, YANG Mu-xin, YUAN Fu-ping, WU Gui-lin, WEI Yu-jie, HUANG Xiao-xu, ZHU Yun-tian. Heterogeneous lamella structure unites ultrafine-grain strength with coarse-grain ductility [J]. Proceedings of the National Academy of Sciences, 2015, 112(47): 14501−14505.

[19] WANG Y F, WANG M S, FANG X T, GUO F J, LIU H Q, SCATTERGOOD R O, HUANG C X, ZHU Y T. Extra strengthening in a coarse/ultrafine grained laminate: Role of gradient interfaces [J]. International Journal of Plasticity, 2019, 123: 196−207.

[20] WANG Yan-fei, YANG Mu-xin, MA Xiao-long, WANG Ming-sai, YIN Kun, HUANG Ai-hui, HUANG Chong-xiang. Improved back stress and synergetic strain hardening in coarse-grain/nanostructure laminates [J]. Materials Science and Engineering A, 2018, 727: 113−118.

[21] YU Tao, LI Feng, WANG Ye, LI Xue-wen. New powder metallurgy preparation method of homogeneous and isomeric Al−Cu−Mg mixed crystal materials [J]. Transactions of Nonferrous Metals Society of China, 2023, 33(2): 371−382.

[22] MAO Qing-zhong, WANG Long, NIE Jin-feng, ZHAO Yong-hao. Enhancing strength and electrical conductivity of Cu−Cr composite wire by two-stage rotary swaging and aging treatments [J]. Composites Part B: Engineering, 2022, 231: 109567.

[23] LI Xin-yu, XIA Wei-jun, CHEN Ji-hua, YAN Hong-ge, LI Zhen-zhen, SU Bin, Min SONG. Dynamic recrystallization, texture and mechanical properties of high Mg content Al−Mg alloy deformed by high strain rate rolling [J]. Transactions of Nonferrous Metals Society of China, 2021, 31(10): 2885−2898.

[24] CHEN Yu-yao, NIE Jin-feng, WANG Fang, YANG Hua-bing, WU Chong-chong, LIU Xiang-fa, ZHAO Yong-hao. Revealing hetero-deformation induced (HDI) stress strengthening effect in laminated Al−$(TiB_2+TiC)_p$/6063 composites prepared by accumulative roll bonding [J]. Journal of Alloys and Compounds, 2020, 815: 152285.

[25] JIANG Lin, YANG H, YEE J K, MO Xuan, TOPPING T, LAVERNIA E J, SCHOENUNG J M. Toughening of aluminum matrix nanocomposites via spatial arrays of boron carbide spherical nanoparticles [J]. Acta Materialia, 2016, 103: 128−140.

[26] ZHAO Yong-feng, MA Xia, CHEN Hou-wen, ZHAO Xiao-jun, LIU Xiang-fa. Preferred orientation and interfacial structure in extruded nano-Al_3BC/6061 Al [J]. Materials & Design, 2017, 131: 23−31.

[27] MA X, ZHAO Y F, TIAN W J, QIAN Z, CHEN H W, WU Y Y, LIU X F. A novel Al matrix composite reinforced by nano-AlN_p network [J]. Scientific Reports, 2016, 6: 34919.

[28] LU Feng-hua, NIE Jin-feng, MA Xia, LI Yu-sheng, JIANG Zhou-wen, ZHANG Yong, ZHAO Yong-hao, LIU Xiang-fa. Simultaneously improving the tensile strength and ductility of the AlN_p/Al composites by the particle's hierarchical structure with bimodal distribution and nano-network [J]. Materials Science and Engineering A, 2020, 770: 138519.

[29] ZHU C Y, HARRINGTON T, GRAY G T, VECCHIO S. Dislocation-type evolution in quasi-statically compressed polycrystalline nickel [J]. Acta Materialia, 2018, 155: 104−116.

[30] GAO H J, HUANG Y G, NIX W D, HUTCHINSON J W. Mechanism-based strain gradient plasticity—I. Theory [J]. Journal of the Mechanics and Physics of Solids, 1999, 47(6): 1239−1263.

[31] KUBIN A L P, MORTENSEN B A. Geometrically necessary dislocations and strain-gradient plasticity: A few critical issues [J]. Scripta Materialia, 2003, 48(2): 119−125.

[32] ZHANG Dong-qing, ZHAO Kai, LI Dao-xiu, REN Lei, LIU Gui-liang, LIU Si-da, LIU Xiang-fa. Microstructure evolution and enhanced mechanical properties in Al−Mn alloy reinforced by B-doped TiC particles [J]. Materials & Design, 2022, 221: 110906.

[33] ZAN Y N, ZHOU Y T, ZHAO H, LIU Z Y, MA Z Y. Enhancing high-temperature strength of $(B_4C+Al_2O_3)$/Al designed for neutron absorbing materials by constructing lamellar structure [J]. Composites Part B: Engineering, 2019, 183: 107674.

[34] SHEN Qiu-yan, YUAN Zhan-wei, LIU Huan, ZHANG Xue-min, FU Qin-qin, WANG Quan-zhao. The damage mechanism of 17vol.%SiC_p/Al composite under uniaxial tensile stress [J]. Materials Science and Engineering A, 2020, 782: 139274.

[35] SHA J J, LV Z Z, LIN G Z, DAI J X, ZU Y F, XIAN Y Q, ZHANG W, CUI D, YAN C L. Synergistic strengthening of aluminum matrix composites reinforced by SiC nanoparticles and carbon fibers [J]. Materials Letters, 2020, 262: 127024.

[36] LI Shi-sheng, SU Yi-shi, JIN Hui-ling, HUANG Yu, OUYANG Qiu-bao, ZHANG Di. Effects of carbon nanotube content on morphology of SiC_p(CNT) hybrid reinforcement and tensile mechanical properties of SiC_p(CNT)/Al composites [J]. Journal of Materials Research, 2017, 32(7): 1239−1247.

[37] GUO Hao, ZHANG Zhong-wu, ZHANG Yang, CUI Ye,

SUN Li-xin, CHEN Dan. Improving the mechanical properties of B_4C/Al composites by solid-state interfacial reaction [J]. Journal of Alloys and Compounds, 2020, 829: 154521.

[38] REDDY M P, UBAID F, SHAKOOR R , PARANDE G, MANAKARI V, MOHAMED A M A, GUPTA M. Effect of reinforcement concentration on the properties of hot extruded Al−Al_2O_3 composites synthesized through microwave sintering process [J]. Materials Science and Engineering A, 2017, 696: 60−69.

[39] KAI Xi-zhou, HUANG Shuo-ming, WU Lin, TAO Ran, PENG Yan-jie, MAO Ze-min, CHEN Fei, LI Gui-rong, CHEN Gang, ZHAO Yu-tao. High strength and high creep resistant ZrB_2/Al nanocomposites fabricated by ultrasonic-chemical in-situ reaction [J]. Journal of Materials Science & Technology, 2019, 35(9): 2107−2114.

[40] KIM W J, YU Y J. The effect of the addition of multiwalled carbon nanotubes on the uniform distribution of TiC nanoparticles in aluminum nanocomposites [J]. Scripta Materialia, 2014, 72/73: 25−28.

[41] NIE Jin-feng, WANG Fang, LI Yu-sheng, LIU Yan-fang, LIU Xiang-fa, ZHAO Yong-hao. Microstructure and mechanical properties of Al−TiB_2/TiC in situ composites improved via hot rolling [J]. Transactions of Nonferrous Metals Society of China, 2017, 27(12): 2548−2554.

[42] TAO Ran, ZHAO Yu-tao, KAI Xi-zhou, ZHAO Zhi-hao, DING Ren-fa, LIANG Liang, XU Wei-tai. Effects of hot rolling deformation on the microstructure and tensile properties of an in situ-generated ZrB_2 nanoparticle-reinforced AA6111 composite [J]. Materials Science and Engineering A, 2018, 732: 138−147.

[43] TAN M J, ZHANG X. Powder metal matrix composites: Selection and processing [J]. Materials Science and Engineering A, 1998, 244: 80−85.

[44] SABIROV I, KOLEDNIK O, VALIEV R Z, PIPPAN R. Equal channel angular pressing of metal matrix composites: Effect on particle distribution and fracture toughness [J]. Acta Materialia, 2005, 53: 4919−4930.

[45] HANSEN N. Hall−Petch relation and boundary strengthening [J]. Scripta Materialia, 2004, 51: 801−806.

[46] YANG Mu-xin, PAN Yue, YUAN Fu-ping, ZHU Yun-tian, WU Xiao-lei. Back stress strengthening and strain hardening in gradient structure [J]. Materials Research Letters, 2016, 4(3): 145−151.

[47] HUANG C X, WANG Y F, MA X L, YIN S, HÖPPEL H W, GöKEN M, WU X L, GAO H J, ZHU Y T. Interface affected zone for optimal strength and ductility in heterogeneous laminate [J]. Materials Today, 2018, 21(7): 713−719.

[48] WANG Y F, HUANG C X, FANG X T, HöPPEL H W, GöKEN M, ZHU Y T. Hetero-deformation induced (HDI) hardening does not increase linearly with strain gradient [J]. Scripta Materialia, 2020, 174: 19−23.

[49] MA Xia, ZHAO Yong-feng, ZHAO Xiao-jun, NIE Jin-feng, CHEN Hou-wen, LIU Xiang-fa. Mechanisms on the outstanding high temperature plasticity of AlN_p/Al−0.4Cu composites induced by cryogenic treatment [J]. Journal of Alloys and Compounds, 2019, 770: 755−764.

[50] NIE Jin-feng, LU Feng-hua, HUANG Zhao-wen, MA Xia, ZHOU Hao, CHEN Cai, CHEN Xiang, YANG Hua-bing, CAO Yang, LIU Xiang-fa, ZHAO Yong-hao, ZHU Yun-tian. Improving the high-temperature ductility of Al composites by tailoring the nanoparticle network [J]. Materialia, 2020, 9: 100523.

[51] KUMAR R V, KESHAVAMURTHY R, PERUGU C S, KOPPAD P G, ALIPOUR M. Influence of hot rolling on microstructure and mechanical behaviour of Al6061−ZrB_2 in-situ metal matrix composites [J]. Materials Science and Engineering A, 2018, 738: 344−352.

通过基体晶粒和颗粒分布异质结构的调控协同提升 AlN_p/Al 复合材料的强度−塑性

陈玉瑶[1]，聂金凤[1]，范 勇[1]，顾 雷[1]，谢可伟[2]，刘相法[2]，赵永好[1]

1. 南京理工大学 材料科学与工程学院 纳米异构材料中心，南京 210094；
2. 山东大学 材料液固结构演变与加工教育部重点实验室，济南 250061

摘 要：为了获得优异的强塑性能，采用液固反应结合后续的热机械处理方法制备了 3 种具有不同微观组织构型的异构 AlN_p/Al 复合材料，详细研究了 AlN 颗粒分布和基体晶粒组织构型对拉伸强度和塑性的影响。结果表明，复合材料的强度和塑性同时提高。其中，具有较弥散颗粒分布的 Uniformed-AlN_p/Al 复合材料表现出优异的极限抗拉强度(~387 MPa)和断裂伸长率(~9.1%)。与其他文献报道的颗粒增强铝基复合材料相比，该复合材料具有较好的比强度和延展性组合。此外，计算了异质变形诱导(HDI)应力。结果表明，在 Uniformed-AlN_p/Al 复合材料中，HDI 应力显著增加。揭示了 HDI 应力在提高 AlN_p/Al 复合材料的强度和塑性中起着至关重要的作用。

关键词：AlN_p/Al 复合材料；拉伸强度；塑性；异质结构；颗粒分布；强化机制

(Edited by Bing YANG)